



## MATHEMATICAL MODELING OF MALARIA AND TYPHOID CO-INFECTION: EXPLORING VECTOR AND NON-VECTOR TRANSMISSION DYNAMICS

QUEENETH OJOMA AHMAN<sup>1,\*</sup>, MARY BASSEY OKOFU<sup>2</sup>,  
CHIOMA LYDIA EJIKEME<sup>2</sup>, EMMANUEL OLORUNFEMI SENEWO<sup>1</sup>  
AND BENEDICT CELESTINE AGBATA<sup>1</sup>

**Abstract.** Malaria and typhoid fever are major infectious diseases that pose significant public health challenges in many parts of the world, particularly in sub-Saharan Africa. This study develops a mathematical model to investigate the dynamics of malaria–typhoid co-infection, incorporating both vector and non-vector malaria transmission routes and environmental transmission for typhoid. Model parameters were drawn from the literature, and simulations were conducted in MATLAB. The results show that vector-borne transmission accounts for over 80% of malaria infections, while typhoid transmission sustains a persistent infection level. Co-infected individuals constitute approximately 25–35% of the total infected population at peak conditions, underscoring the substantial burden of simultaneous infection. Sensitivity analysis identifies malaria and typhoid transmission rates as key drivers of co-infection prevalence. A backward bifurcation in the malaria subsystem indicates that malaria may persist even when its reproduction number is below one, thereby continually seeding co-infection and indirectly maintaining typhoid transmission through co-infected individuals. These findings highlight the need for integrated and sustained control strategies, including vector control, typhoid vaccination, and improved sanitation, to effectively reduce the dual disease burden. Overall, the model provides a useful analytical framework to support public health planning and evidence-based resource allocation in regions where both infections remain endemic.

**Mathematics Subject Classification.** 92D30, 92D25, 37N25, 65M70, 91B06.

Received August 30, 2025. Accepted February 2, 2026.

### 1. INTRODUCTION

Malaria and typhoid fever continue to pose serious public health challenges across many tropical regions, particularly in sub-Saharan Africa and parts of South Asia. These diseases are not only highly prevalent but frequently co-exist in communities affected by poverty, inadequate sanitation, and limited access to quality healthcare [1–5]. In such environments, the occurrence of malaria–typhoid coinfection is increasingly common, leading to diagnostic confusion and treatment complications due to overlapping symptoms such as fever, chills,

---

*Keywords and phrases:* Reproduction number, bifurcation analysis, partial rank correlation coefficient, sensitivity analysis, epidemiological modeling.

<sup>1</sup> Department of Mathematics and Statistics, Confluence University of Science and Technology, Osara, Nigeria.

<sup>2</sup> Department of Mathematics, University of Nigeria Nsukka, Nsukka, Nigeria.

\* Corresponding author: [ahmanqo@custech.edu.ng](mailto:ahmanqo@custech.edu.ng)

abdominal pain, and fatigue [6–10]. Malaria and typhoid fever are two of the most common febrile illnesses in sub-Saharan Africa, and their co-occurrence poses diagnostic and treatment challenges. Several studies have documented the prevalence and clinical implications of malaria–typhoid co-infection in Nigeria [11–13].

Malaria, primarily caused by the *Plasmodium falciparum* parasite, is commonly transmitted through the bites of infected female *Anopheles* mosquitoes. However, research has shown that malaria can also spread through non-vector routes—such as blood transfusions, shared needles and organ transplants. These non-mosquito pathways are particularly relevant in healthcare settings and densely populated urban environments where vector exposure may not be the only route of infection [14–18].

On the other hand, typhoid fever is a bacterial infection caused by *Salmonella enterica* serovar Typhi, often spread through the ingestion of food or water contaminated with fecal matter. In areas where sanitation infrastructure is inadequate, typhoid can spread rapidly. Although it is both preventable and treatable, poor health systems and rising antibiotic resistance continue to sustain the disease burden in many low-resource communities [19–21].

The implications of malaria–typhoid coinfection are particularly concerning. Studies have found that the interaction of both pathogens in a single host can worsen disease severity, impair immune responses, and increase the likelihood of complications such as organ failure or death. From a healthcare system perspective, coinfections result in prolonged hospitalizations, increased treatment costs, and challenges in disease surveillance and control [22, 23].

Mathematical modeling has long played a vital role in epidemiology by helping researchers understand disease dynamics, evaluate intervention strategies, and simulate outbreak scenarios. Several mathematical models have been developed for malaria and typhoid individually, and more recently, for their coinfection [24, 25]. However, most of these models focus on traditional vector-borne transmission of malaria and do not incorporate non-vector routes, potentially underestimating the actual transmission dynamics—especially in modern clinical or urban settings.

This study introduces a novel deterministic compartmental model for malaria and typhoid fever coinfection that uniquely integrates both vector and non-vector transmission pathways for malaria. The model also includes distinct compartments for individuals infected with only one of the diseases or both, allowing for a more accurate representation of coinfection dynamics. This addition is particularly crucial for reflecting the epidemiological realities in environments such as healthcare facilities or urban settlements, where multiple transmission pathways coexist.

The primary objectives of this study are to:

1. Develop a biologically realistic model that incorporates both vector and non-vector malaria transmission pathways in the presence of typhoid;
2. Derive and interpret the basic reproduction number ( $R_0$ ) for the system;
3. Analyze the stability of both the disease-free and endemic equilibria;
4. Conduct sensitivity analysis to determine which parameters most significantly influence disease spread;
5. Perform numerical simulations to assess the potential effectiveness of various intervention strategies.

By addressing the dual modes of malaria transmission in the context of typhoid fever, this model aims to offer new insights into coinfection dynamics and support the development of targeted control strategies in affected regions.

In this study, we present a malaria–typhoid co-infection model that integrates both vector and non-vector malaria transmission pathways together with environmental typhoid transmission, while also incorporating seasonal variation in malaria transmission intensity. Unlike previous co-infection models that treat the two diseases in isolation or without environmental contamination, our formulation explicitly captures the interaction between infection pathways through co-infected individuals and the bacteria reservoir. This framework allows us to examine how malaria persistence, particularly under seasonal forcing and backward bifurcation conditions, influences the maintenance of typhoid infection and co-infection burdens. The analytical results and simulations therefore provide new insight into how integrated interventions targeting both malaria and typhoid are more effective than disease-specific control strategies applied independently.

The novelty of this study lies in the simultaneous incorporation of (i) dual malaria transmission pathways (vector-mediated and non-vector-mediated), (ii) environmental transmission of typhoid through a dynamic bacterial reservoir, (iii) explicit co-infection progression mechanisms linking the two diseases, and (iv) seasonal forcing in the mosquito-to-human transmission rate. These features are not jointly represented in existing malaria–typhoid co-infection models. By integrating these components in a unified framework, this work provides new insight into how seasonal malaria persistence and co-infection feedbacks can sustain typhoid circulation and increase overall disease burden, thereby highlighting the need for coordinated rather than disease-specific intervention strategies.

## 2. METHODS

This section presents the formulation and analysis of a deterministic compartmental model designed to capture the transmission dynamics of malaria and typhoid fever co-infection within a human population. The model integrates both vector-mediated and non-vector-mediated transmission routes, along with the environmental persistence of typhoid bacteria. Ordinary differential equations (ODEs) are employed to describe the time evolution of each compartment.

### 2.1. Malaria and typhoid mathematical model formulation

This study develops a deterministic compartmental model to describe the transmission dynamics and interactions between malaria and typhoid infections in a human population. The model incorporates both vector-borne and non-vector-borne transmission pathways for malaria, alongside environmental transmission of typhoid through a bacterial reservoir. It divides the total human population into seven epidemiological compartments, which include susceptible individuals, individuals infected with malaria only (*via* both mosquito and non-vector pathways), individuals infected with typhoid only (*via* bacterial reservoir), co-infected individuals, treated individuals, and those recovered with temporary immunity.

Additionally, the model accounts for the mosquito vector population involved in malaria transmission, consisting of uninfected and infected classes. It also incorporates a compartment representing the concentration of typhoid-causing bacteria in the environment, which plays a role in the transmission of typhoid to humans.

Transitions between compartments are governed by a system of nonlinear ordinary differential equations (ODEs), and the model captures key features such as co-infection dynamics, treatment, recovery, loss of immunity, and natural and disease-induced mortality. The model is designed to reflect disease patterns in regions where both malaria and typhoid fever are endemic and co-infections are common.

It should be noted that the malaria vector-to-human transmission rate is seasonal and is represented as  $\lambda_{m1}(t) = \lambda_{m1,0} \left(1 + \alpha \sin\left(\frac{2\pi t}{12}\right)\right)$ , which introduces a periodic (non-autonomous) element into the model. For analytical tractability in the derivation of equilibrium points and reproduction numbers, the time-averaged value  $\lambda_{m1,0}$  is used in the autonomous reduction of the system, while numerical simulations utilize the full seasonal form.

The following presents the model assumptions, flow diagram, system of equations, and descriptions of model variables and parameters.

#### 2.1.1. Malaria and typhoid coinfection model assumptions

The construction of the malaria-typhoid co-infection model relies on the following key assumptions, consistent with established models in epidemiological research:

1. **Constant Recruitment:** It is assumed that the human population, vector population and bacterial reservoir are replenished at constant recruitment rates. This is a common assumption to maintain demographic balance and population stability over time [26, 27].

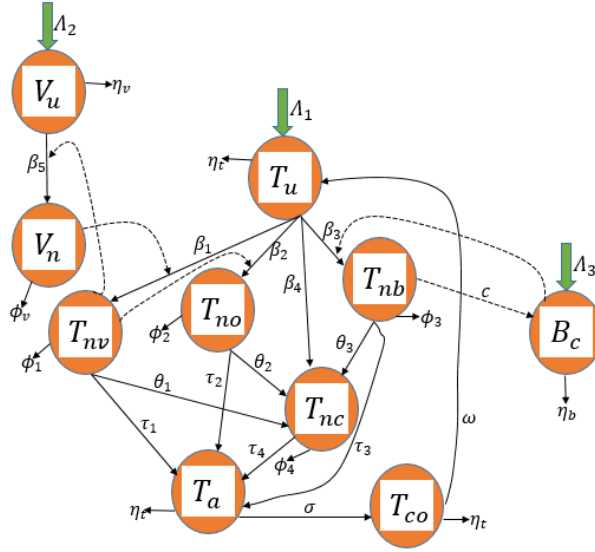


FIGURE 1. Malaria and typhoid coinfection flow diagram.

2. **No Vertical Transmission:** Both malaria and typhoid are assumed to be transmitted horizontally only. No mother-to-child or vector transovarial transmission is included in this model. Any references to vertical transmission in the introduction are meant as general biological background and do not apply to the present system [28].
3. **Homogeneous Mixing:** All individuals in the human and vector populations are assumed to mix homogeneously, so each susceptible individual has an equal probability of becoming infected upon contact [26, 29].
4. **Co-Infection Pathways:** Individuals can become co-infected either through sequential exposure (*i.e.*, malaria followed by typhoid or vice versa) or simultaneously through overlapping exposure [28, 30].
5. **Temporary Immunity:** Individuals who recover from treatment enter a recovered class where they experience temporary immunity and eventually return to the susceptible class after immunity wanes [31, 32].
6. **Disease-Induced Mortality:** Infections may result in disease-induced mortality for malaria only, typhoid only, and co-infection [29, 33].
7. **Typhoid Reservoir Contribution:** Typhoid-infected individuals contribute to the bacterial reservoir, increasing the environmental contamination level and facilitating further infections [30].
8. **No Super-Infection:** The model excludes the possibility of individuals being infected by the same pathogen more than once at the same time, allowing only single or dual infection with one malaria strain and typhoid [28].
9. **Malaria Non-vector Transmission:** Malaria can be transmitted through vector and non-vector pathways in the model [14].
10. **Seasonal variation:** The vector-borne transmission rate is assumed to vary seasonally, reflecting climatic influences such as rainfall, humidity, and temperature. This is modeled using a sinusoidal function with a 12-month period, consistent with malaria seasonality in endemic regions [34, 35].

### 2.1.2. Malaria and typhoid coinfection model flow diagram

In this subsection, we present the flow diagram of the malaria and typhoid coinfection model, which serves as a visual representation of the key compartments and interactions within the system. The model accounts for both vector and non-vector transmission pathways for malaria, as well as the role of a bacterial reservoir in the transmission of typhoid. The flow diagram in Figure 1 illustrates the dynamics between susceptible, infected, co-infected, treated, and recovered individuals, providing a foundation for the subsequent mathematical formulation and simulation.

Here;

$$\left. \begin{aligned} \beta_1(t) &= \lambda_{m1}(t) \cdot V_n, \text{ where} \\ \lambda_{m1}(t) &= \lambda_{m1,0} \left( 1 + \alpha \sin \left( \frac{2\pi t}{12} \right) \right), \\ \beta_2 &= \lambda_{m2} T_{nv}, \beta_3 = \lambda_t B_c, \\ \beta_4 &= \beta_1(t) + \beta_2 + \beta_3 = \lambda_{m1} V_n + \lambda_{m2} T_{nv} + \lambda_t B_c, \\ \beta_5 &= \lambda_v T_{nv}, \phi_1 = \eta_t + \gamma_m, \phi_2 = \eta_t + \gamma_m, \\ \phi_3 &= \eta_t + \gamma_t, \phi_4 = \eta_t + \gamma_m + \gamma_t, \phi_v = \eta_v + \gamma_v \end{aligned} \right\}. \quad (2.1)$$

The seasonal variation in the mosquito–human contact rate is modeled as:

$$\lambda_{m1}(t) = \lambda_{m1,0} \left( 1 + \alpha \sin \left( \frac{2\pi t}{12} \right) \right), \quad (2.2)$$

where  $\lambda_{m1,0}$  is the mean contact rate,  $\alpha$  is the amplitude of seasonal variation ( $0 < \alpha < 1$ ), and  $t$  is time in months. The corresponding vector-borne transmission rate is given by:

$$\beta_1(t) = \lambda_{m1}(t) \cdot V_n. \quad (2.3)$$

Figure 14 illustrates the seasonal forcing in  $\lambda_{m1}(t)$ .

Although  $\lambda_{m1}(t)$  may vary seasonally, all equilibrium and reproduction number analyses assume it is constant. Time dependence is reintroduced only during the seasonal forcing simulations.

### 2.1.3. Malaria and typhoid coinfection model equations

This subsection outlines the mathematical formulation of the malaria and typhoid coinfection model. The system of differential equations is derived to describe the interactions between the compartments introduced in the flow diagram Figure 1, capturing the dynamics of both diseases. The equations account for the transmission of malaria *via* both vector and non-vector pathways, as well as the bacterial transmission dynamics of typhoid. Key parameters, such as transmission rates, recovery rates, and treatment effects, are incorporated to provide a comprehensive framework for analyzing the coinfection dynamics. These equations will serve as the foundation

for model simulations and further analytical studies.

$$\left. \begin{aligned}
 (a) \quad & \frac{dT_u}{dt} = \Lambda_1 + \rho T_{co} - (\eta_t + \beta_1(t) + \beta_2 + \beta_3 + \beta_4)T_u \\
 (b) \quad & \frac{dT_{nv}}{dt} = \beta_1(t)T_u - (\phi_1 + \theta_1 + \tau_1)T_{nv} \\
 (c) \quad & \frac{dT_{no}}{dt} = \beta_2 T_u - (\phi_2 + \theta_2 + \tau_2)T_{no} \\
 (d) \quad & \frac{dT_{nb}}{dt} = \beta_3 T_u - (\phi_3 + \theta_3 + \tau_3)T_{nb} \\
 (e) \quad & \frac{dT_{nc}}{dt} = \beta_4 T_u + \theta_1 T_{nv} + \theta_2 T_{no} + \theta_3 T_{nb} - (\phi_4 + \tau_4)T_{nc} \\
 (f) \quad & \frac{dT_a}{dt} = \tau_1 T_{nv} + \tau_2 T_{no} + \tau_3 T_{nb} + \tau_4 T_{nc} - (\eta_t + \sigma)T_a \\
 (g) \quad & \frac{dT_{co}}{dt} = \sigma T_a - (\eta_t + \rho)T_{co} \\
 (h) \quad & \frac{dV_u}{dt} = \Lambda_2 - (\eta_v + \beta_5)V_u \\
 (i) \quad & \frac{dV_n}{dt} = \beta_5 V_u - \phi_v V_n \\
 (j) \quad & \frac{dB_c}{dt} = \Lambda_3 + cT_{nb} - \eta_b B_c
 \end{aligned} \right\} \quad (2.4)$$

$$\left. \begin{aligned}
 T_u(0) > 0, \quad T_{nv}(0) \geq 0, \quad T_{no}(0) \geq 0, \quad T_{nb}(0) \geq 0, \\
 T_{nc}(0) \geq 0, \quad T_a(0) \geq 0, \quad T_{co}(0) \geq 0, \\
 V_u(0) \geq 0, \quad V_n(0) \geq 0, \quad B_c(0) \geq 0
 \end{aligned} \right\}. \quad (2.5)$$

#### 2.1.4. Malaria and typhoid coinfection model variables and parameters description

In this subsection, we in Table 1 provide a detailed description of the variables and parameters used in the malaria and typhoid coinfection model. Each variable represents a compartment or state within the system, such as susceptible, infected, or recovered individuals for both malaria and typhoid. The parameters define the rates of transmission, recovery, and other key processes, including the rate of treatment and shedding of infectious bacteria into the bacterial reservoirs. Understanding these variables and parameters is crucial for the interpretation of the model dynamics and the subsequent analysis of the coinfection system.

## 2.2. Malaria and typhoid coinfection model analysis

This section presents a theoretical analysis of the malaria-typhoid co-infection model. The goal is to ensure that the model is epidemiologically and mathematically well-posed, identify its equilibria, and examine the stability of the malaria and typhoid coinfection disease-free equilibrium and also obtain the model Reproduction number using the next-generation matrix approach.

### 2.2.1. Positivity and boundedness of solutions

For any epidemiological model such as equation (2.4), it is crucial to demonstrate that the solutions remain both non-negative and bounded over time, ensuring biological feasibility. This guarantees that the model's variables representing population subgroups do not attain negative values or grow without bound, which would be unrealistic.

TABLE 1. Malaria and typhoid coinfection model variables description.

Variables	Description
$T_u$	Susceptible Uninfected human population
$T_{nv}$	Humans infected with malaria <i>via</i> vector
$T_{no}$	Humans infected with malaria <i>via</i> non-vector route
$T_{nb}$	Humans infected with typhoid only
$T_{nc}$	Humans co-infected with both malaria and typhoid
$T_a$	Treated individuals
$T_{co}$	Temporarily immune recovered individuals
$V_u$	Susceptible Uninfected mosquito vectors
$V_n$	Infected mosquito vectors
$B_c$	Typhoid bacterial reservoir in environment

TABLE 2. Parameters for the malaria–typhoid co-infection model.

Parameter	Description	Value per week	Reference
<i>Demographic and Environmental Parameters</i>			
$\Lambda_1$	Recruitment rate into human population	20	[22]
$\Lambda_2$	Recruitment rate into vector population	100	[22]
$\Lambda_3$	Input rate into environmental bacteria reservoir	50	[30]
$\eta_h$	Natural death rate (humans)	$1.0 \times 10^{-3}$	[36]
$\eta_v$	Natural death rate (mosquitoes)	0.05	[37]
$\eta_b$	Environmental bacteria decay rate	0.10	[38]
<i>Transmission Parameters</i>			
$\lambda_{m1,0}$	Baseline mosquito-to-human malaria transmission rate	Fitted	[39]
$\alpha$	Amplitude of seasonal forcing (dimensionless)	0.5	Assumed
$\lambda_{m1}(t)$	Seasonal malaria transmission rate	See equation (3)	This study
$\lambda_{m2}$	Non-vector malaria transmission rate	$1.2 \times 10^{-2}$	[28]
$\lambda_t$	Typhoid transmission rate (human/environment)	$3.0 \times 10^{-2}$	[38]
$c$	Bacteria shedding rate (typhoid infectives)	$5.0 \times 10^{-2}$	[38]
<i>Progression and Treatment Parameters</i>			
$\theta_1$	Malaria (vector) $\rightarrow$ co-infection progression	0.01	[28]
$\theta_2$	Malaria (non-vector) $\rightarrow$ co-infection progression	0.005	[28]
$\theta_3$	Typhoid $\rightarrow$ co-infection progression	0.007	[30]
$\tau_1$	Treatment rate for vector malaria	0.10	[40]
$\tau_2$	Treatment rate for non-vector malaria	0.08	[40]
$\tau_3$	Treatment rate for typhoid	0.09	[30, 41]
$\tau_4$	Treatment rate for co-infection	0.07	Assumed
<i>Recovery, Immunity, and Disease-Induced Mortality</i>			
$\sigma$	Recovery rate to temporary immunity	0.10	[40]
$\omega$	Loss of immunity rate	0.01	Assumed
$\gamma_m$	Malaria-induced mortality (humans)	$1.0 \times 10^{-3}$	[36]
$\gamma_t$	Typhoid-induced mortality (humans)	$5.0 \times 10^{-4}$	[36]
$\gamma_v$	Disease-induced mortality (mosquitoes)	0.02	[37]

### Positivity of solutions

Considering the initial conditions in equation (2.4). We consider the domain as The feasible region is defined as:

$$\Omega_c = \{ ( T_u, T_{nv}, T_{no}, T_{nb}, T_{nc}, T_a, T_{co}, V_u, V_n, B_c ) \in \mathbb{R}_+^{10} \}$$

We observe that all the equations in the system equation (2.4) are of the form:

$$\frac{dX}{dt} = \text{recruitment term} - \text{non-negative loss terms.}$$

As such, they conform to the standard structure where each variable's rate of change is a balance of inflow and outflow, and the outflow terms are proportional to the variable itself. Applying the comparison theorem, we find that each compartment remains non-negative for all  $t > 0$ .

For example, consider the susceptible uninfected human class  $T_u$  in equation (2.4)(a). The right-hand side is linear in  $T_u$ , and since  $\Lambda_1 > 0$  and all loss terms are non-negative, solutions to this equation remain positive for all  $t \geq 0$ , provided  $T_u(0) > 0$ .

The same argument holds for all other compartments using Gronwall's inequality and the non-negativity of parameters and initial conditions.

### Boundedness of solutions

To demonstrate boundedness, we consider the total human population:

$$H_t(t) = T_u + T_{nv} + T_{no} + T_{nb} + T_{nc} + T_a + T_{co}$$

Taking the derivative and summing all human equations:

$$\frac{dH_t}{dt} = \Lambda_1 - \eta_t H_t$$

Solving this differential inequality gives:

$$H_t(t) \leq H_t(0)e^{-\eta_t t} + \frac{\Lambda_1}{\eta_t} (1 - e^{-\eta_t t})$$

As  $t \rightarrow \infty$ , we get:

$$\lim_{t \rightarrow \infty} H_t(t) \leq \frac{\Lambda_1}{\eta_t}$$

Thus, the total human population is bounded by the recruitment rate and the natural death rate. Similarly, for the vector population:

$$H_v(t) = V_u + V_n \frac{dH_v}{dt} = \Lambda_2 - \eta_v H_v$$

Solving we have; Solving the inequality for the total vector population, we get: Solving the inequality for the total vector population, we get:

$$H_v(t) \leq H_v(0) e^{-\eta_v t} + \frac{\Lambda_2}{\eta_v} (1 - e^{-\eta_v t})$$

To demonstrate boundedness, we also consider the total vector population. The total vector population satisfies the inequality:

$$H_v(t) \leq H_v(0) e^{-\eta_v t} + \frac{\Lambda_2}{\eta_v} (1 - e^{-\eta_v t})$$

As  $t \rightarrow \infty$ , we obtain:

$$\lim_{t \rightarrow \infty} H_v(t) \leq \frac{\Lambda_2}{\eta_v}$$

$$\lim_{t \rightarrow \infty} H_v(t) \leq \frac{\Lambda_2}{\eta_v}$$

Thus, the total vector population is bounded by its recruitment and natural death rates. As  $t \rightarrow \infty$ , we have:

$$\lim_{t \rightarrow \infty} H_v(t) \leq \frac{\Lambda_2}{\eta_v}$$

Thus, the total vector population is bounded by its recruitment and natural death rates. Similarly, for the bacterial population:

$$H_b(t) = B_c$$

$$\frac{dH_b}{dt} = A_3 - \eta_b H_b$$

Solving we have;

$$H_b(t) \leq H_b(0) e^{\eta_b t} + \frac{A_3}{\eta_b} (1 - e^{\eta_b t})$$

$$\text{As } t \rightarrow \infty,$$

we get:

$$\lim_{t \rightarrow \infty} H_b(t) \leq \frac{A_3}{\eta_b}.$$

Thus, the total bacterial population is bounded by source and decay. Therefore, all compartments remain bounded by source and decay for all finite  $t \geq 0$ , and the solutions of the system are ultimately contained in a

compact, positively invariant region of  $\mathbb{R}_+^{10}$ . The model is thus epidemiologically and mathematically well-posed, with solutions that are both non-negative and uniformly bounded in  $\Omega_c$  for all  $t \geq 0$ , given non-negative initial conditions. This validates the system as a reliable representation of the co-infection dynamics of malaria and typhoid.

### 2.2.2. Malaria and typhoid coinfection model equilibrium points

Here, we determine the equilibrium points of the malaria and typhoid coinfection model formulated. Equilibrium points represent the states at which the population distribution among the compartments remains constant over time. These are obtained by setting the right-hand sides of all differential equations in the model equation (2.4) to zero and solving the resulting system of algebraic equations.

For this model we consider two types of equilibrium points:

1. The **Disease-Free Equilibrium (DFE)**, where there is no malaria and typhoid infection present in the population (*i.e.*, all infected compartments are zero).
2. The **Endemic Equilibrium (EE)**, where the malaria and typhoid disease persists in the population with one or more infected compartments maintaining positive values.

The equilibrium analysis provides a basis for understanding the conditions under which the malaria and typhoid diseases either die out or persist.

#### *Malaria and typhoid coinfection model disease-free equilibrium ( $Q_0$ )*

The malaria and typhoid coinfection model Disease-Free Equilibrium ( $Q_0$ ) corresponds to the state where no individual in the population is infected with either malaria, typhoid, or both. This implies that all the infection-related compartments in the model are equal to zero at equilibrium. At this equilibrium state, we assume that only the susceptible compartments are non-zero, and the system remains in a steady state.

To find  $Q_0$ , we set the derivatives of all state variables in the model (2.4) to zero and assume the infected compartments are zero. That is:

$$T_{nv} = T_{no} = T_{nb} = T_{nc} = T_a = T_{co} = V_n = c = 0$$

We substitute these into the system of equation (2.4) and solve for the remaining variables:  
From the susceptible human equation:

$$\begin{aligned} 0 &= A_1 + \rho T_{co} - (\eta_t + \beta_1(t) + \beta_2 + \beta_3 + \beta_4) T_u \\ &\Rightarrow T_u^0 = \frac{A_1}{\eta_t} \end{aligned}$$

From the uninfected vector equation:

$$\begin{aligned} 0 &= A_2 - (\eta_v + \beta_5) V_u \\ &\Rightarrow V_u^0 = \frac{A_2}{\eta_v} \end{aligned}$$

From the bacterial equation:

$$\begin{aligned} 0 &= A_3 + c T_{nb} - \eta_b B_c \\ &\Rightarrow B_c^0 = \frac{A_3}{\eta_b} \end{aligned}$$

Thus, the model disease-free equilibrium ( $Q_0$ ) is given by:

$$\begin{aligned} Q_0 &= \{T_u^0, T_{nv}^0, T_{no}^0, T_{nb}^0, T_{nc}^0, T_a^0, T_{co}^0, V_u^0, V_n^0, B_c^0\} \\ &= \left\{ \frac{\Lambda_1}{\eta_t}, 0, 0, 0, 0, 0, 0, \frac{\Lambda_2}{\eta_v}, 0, \frac{\Lambda_3}{\eta_b} \right\}. \end{aligned}$$

This equilibrium point represents a scenario where the entire population is uninfected, and the system is maintained by the recruitment rates in the human, vector, and environmental bacterial compartments respectively. The stability of this equilibrium will be analyzed in subsequent sections to determine the conditions under which the diseases can be eradicated.

### *Malaria and typhoid coinfection model endemic equilibrium ( $Q_1$ )*

At the malaria and typhoid coinfection model endemic equilibrium point ( $Q_1$ ), all the model compartments are non-zero, including those for infected individuals. This implies that these diseases persist in the population. This equilibrium point is found by solving the system of equations in steady state simultaneously:

Let:

$$Q_1 = \{T_u^*, T_{nv}^*, T_{no}^*, T_{nb}^*, T_{nc}^*, T_a^*, T_{co}^*, V_u^*, V_n^*, B_c^*\}.$$

Equating all the derivatives in equation (2.4) to zero and solving simultaneously we obtained the following;

$$\left. \begin{aligned} T_{nv}^* &= \frac{\beta_1(t)T_u^*}{K_2}, & T_{no}^* &= \frac{\beta_2 T_u^*}{K_3}, & T_{nb}^* &= \frac{\beta_3 T_u^*}{K_4}, \\ T_{nc}^* &= \frac{XT_u^*}{K_5}, & T_a^* &= \frac{YT_u^*}{K_6}, & T_{co}^* &= \frac{\sigma Y T_u^*}{K_6 K_7}, \\ T_u^* &= \frac{\Lambda_1 K_1 K_6 K_7}{K_1 K_6 K_7 - \rho Y}, & V_u^* &= \frac{\Lambda_2}{K_8}, & V_n^* &= \frac{\beta_5 \Lambda_2}{K_8 K_9}, \\ B_c^* &= \frac{K_4 \Lambda_3 + c \beta_3 T_u^*}{K_4 K_{10}} \end{aligned} \right\} \quad (2.6)$$

Where;

$$\left. \begin{aligned} K_1 &= \eta_t + \beta_1(t) + \beta_2 + \beta_3 + \beta_4, \\ K_2 &= \phi_1 + \theta_1 + \tau_1, & K_3 &= \phi_2 + \theta_2 + \tau_2, \\ K_4 &= \phi_3 + \theta_3 + \tau_3, & K_5 &= \phi_4 + \tau_4, \\ K_6 &= \eta_t + \sigma, & K_7 &= \eta_t + \rho, & K_8 &= \phi_v, \\ K_9 &= \eta_v + \beta_5, & K_{10} &= \eta_b, \\ X &= \left( \beta_4 + \frac{\beta_1(t)\theta_1}{K_2} + \frac{\beta_2\theta_2}{K_3} + \frac{\beta_3\theta_3}{K_4} \right) \frac{T_u^*}{K_5}, \\ Y &= \left( \frac{\beta_1(t)\tau_1}{K_2} + \frac{\beta_2\tau_2}{K_3} + \frac{\beta_3\tau_3}{K_4} + \frac{X\tau_4}{K_5} \right) \frac{T_u^*}{K_6} \end{aligned} \right\}. \quad (2.7)$$

Therefore, the malaria and typhoid coinfection model (2.4) admits a biologically feasible endemic equilibrium point, which represents the steady-state situation where malaria and typhoid infections persist in the population. This result provides a foundation for further analysis, including the computation of the basic reproduction number and investigation of the stability of the endemic state.

### 2.2.3. Calculation of malaria and typhoid coinfection basic reproduction number ( $R_{mt}$ )

In understanding how diseases spread within a population, one of the most important indicators is the Basic Reproduction Number. Essentially, it tells us how contagious a disease is. Specifically, it represents the average number of people that one infected individual will pass the disease to in a fully susceptible population. For infectious diseases like malaria and typhoid, which can often occur together as a coinfection,  $R_{mt}$  helps us predict whether the diseases will spread, how quickly they might do so, and the impact they may have on the community.

The Next-Generation Matrix Method [27] is a mathematical tool used to calculate  $R_{mt}$  in complex disease models like this one, where multiple diseases (in this case, malaria and typhoid) interact. In such models, different compartments represent different states of infection like uninfected individuals, those infected with malaria or typhoid, and individuals with both diseases. To find  $R_{mt}$ , we focus on the infection terms, which describe how one disease spreads to others, and the transition terms, which capture how individuals move between different infection states.

By constructing two matrices;  $U$ , which contains the terms that describe how new infections are introduced, and  $Z$ , which captures the rates of individuals transitioning between different infection states we can compute  $R_{mt}$ . This gives us the dominant eigenvalue of the matrix  $UZ^{-1}$ , which provides a single, powerful number that quantifies the potential for malaria and typhoid to spread within the population.

Here we will use the Next-Generation Matrix Method to calculate  $R_{mt}$  for the model dynamic system (2.4) of malaria and typhoid coinfection. By breaking down the key steps identifying the infection and transition terms, constructing the matrices, and calculating  $R_{mt}$  we'll get a clearer picture of how these diseases interact and the likelihood of their spread in a population. For the malaria and typhoid coinfection model equation (2.4), the key compartments involved in the disease dynamics are:

$$T_{nv}, T_{no}, T_{nb}, T_{nc}, T_a, V_n, B_c$$

Given these compartments, we proceed with the construction of matrices as follows;

$$U = \begin{bmatrix} \beta_1(t)T_u \\ \beta_2T_u \\ \beta_3T_u \\ \beta_4T_u \\ 0 \\ \beta_5V_u \\ 0 \end{bmatrix}, \quad Z = \begin{bmatrix} K_2T_{vn} \\ K_3T_{no} \\ K_4T_{nb} \\ K_5T_{nc} - \theta_1T_{vn} - \theta_2T_{n0} - \theta_3T_{nb} \\ K_6T_a - \tau_1T_{vn} - \tau_2T_{n0} - \tau_3T_{nb} - \tau_4T_{nc} \\ K_9V_n \\ K_{10}B_c - cT_{nb} \end{bmatrix}$$

$$U = \begin{bmatrix} 0 & 0 & 0 & 0 & 0 & d_1 & 0 \\ d_2 & 0 & 0 & 0 & 0 & 0 & 0 \\ 0 & 0 & 0 & 0 & 0 & 0 & d_3 \\ d_4 & 0 & 0 & 0 & 0 & d_5 & d_6 \\ 0 & 0 & 0 & 0 & 0 & 0 & 0 \\ d_7 & 0 & 0 & 0 & 0 & 0 & 0 \\ 0 & 0 & 0 & 0 & 0 & 0 & 0 \end{bmatrix}$$

$$Z = \begin{bmatrix} K_2 & 0 & 0 & 0 & 0 & 0 & 0 \\ 0 & K_3 & 0 & 0 & 0 & 0 & 0 \\ 0 & 0 & K_4 & 0 & 0 & 0 & 0 \\ -a & -b & -c & K_5 & 0 & 0 & 0 \\ -d & -e & -f & -g & K_6 & 0 & 0 \\ 0 & 0 & 0 & 0 & 0 & K_9 & 0 \\ 0 & 0 & -h & 0 & 0 & 0 & K_{10} \end{bmatrix}$$

Where;

$$\left. \begin{aligned} a &= \theta_1, & b &= \theta_2, & c &= \theta_3, & d &= \tau_1, \\ e &= \tau_2, & f &= \tau_3, & g &= \tau_4, & h &= c, \\ d_1 &= \frac{\lambda_{m1}A_1}{\eta_t}, & d_2 &= \frac{\lambda_{m2}A_1}{\eta_t}, & d_3 &= \frac{\lambda_t A_1}{\eta_t}, \\ d_4 &= \frac{\lambda_{m2}A_1}{\eta_t}, & d_5 &= \frac{\lambda_{m1}A_1}{\eta_t}, & d_6 &= \frac{\lambda_t A_1}{\eta_t}, \\ d_7 &= \frac{\lambda_v A_2}{\eta_v} \end{aligned} \right\}. \quad (2.8)$$

Using MATLAB software, we compute  $UZ^{-1}$  as follows:

$$Z^{-1} = \begin{bmatrix} \frac{1}{K_2} & 0 & 0 & 0 & 0 & 0 & 0 \\ 0 & \frac{1}{K_2} & 0 & 0 & 0 & 0 & 0 \\ 0 & 0 & \frac{1}{K_2} & 0 & 0 & 0 & 0 \\ \frac{a}{K_5 K_2} & \frac{b}{K_5 K_3} & \frac{c}{K_5 K_4} & \frac{1}{K_5} & 0 & 0 & 0 \\ \frac{K_5 d + ga}{K_6 K_5 K_2} & \frac{K_5 e + gb}{K_6 K_5 K_3} & \frac{K_5 f + gc}{K_6 K_5 K_4} & \frac{g}{K_5 K_6} & \frac{1}{K_6} & 0 & 0 \\ 0 & 0 & 0 & 0 & 0 & \frac{1}{K_9} & 0 \\ 0 & 0 & \frac{h}{K_{10} K_4} & 0 & 0 & 0 & \frac{1}{K_{10}} \end{bmatrix}$$

$$UZ^{-1} = \begin{bmatrix} 0 & 0 & 0 & 0 & 0 & \frac{d_1}{K_9} & 0 \\ \frac{d_2}{K_2} & 0 & 0 & 0 & 0 & 0 & 0 \\ 0 & 0 & \frac{d_3 h}{K_{10} K_4} & 0 & 0 & 0 & \frac{d_3}{K_{10}} \\ \frac{d_4}{K_2} & 0 & \frac{d_6 h}{K_{10} K_4} & 0 & 0 & \frac{d_5}{K_9} & \frac{d_6}{K_{10}} \\ 0 & 0 & 0 & 0 & 0 & 0 & 0 \\ \frac{d_7}{K_2} & 0 & 0 & 0 & 0 & 0 & 0 \\ 0 & 0 & 0 & 0 & 0 & 0 & 0 \end{bmatrix}.$$

Using MATLAB software, we compute the eigenvalue of  $UZ^{-1}$  as follows;

$$eig(UZ^{-1}) = \begin{bmatrix} 0 \\ 0 \\ 0 \\ 0 \\ \frac{d_3 h}{K_{10} K_4} \\ + \sqrt{\frac{d_1 d_7}{K_2 K_9}} \\ - \sqrt{\frac{d_1 d_7}{K_2 K_9}} \end{bmatrix}.$$

The Basic Reproduction Number  $R_{mt}$  is the largest eigenvalue, From the eigenvalues of the next-generation matrix product  $UZ^{-1}$ , we obtain two key quantities:

$R_m = \sqrt{\frac{d_1 d_7}{K_2 K_9}}$  – which represents the basic reproduction number for malaria infection in the model.

$R_t = \frac{d_3 h}{K_{10} K_4}$  – which represents the basic reproduction number for typhoid infection in the model.

Thus,

$$R_m = \sqrt{\frac{\lambda_{m1} \lambda_v A_1 A_2}{\eta_t \eta_v^2 (\eta_t + \gamma_m + \theta_1 + \tau_1)}} \quad \text{and} \quad R_t = \frac{\lambda_t A_1 c}{\eta_b (\eta_t + \gamma_t + \theta_3 + \tau_3)}.$$

These values correspond to the dominant contributions to disease transmission from the malaria only and typhoid only transmission cycles within the coinfection framework.

The overall basic reproduction number for the malaria-typhoid coinfection model, denoted by  $R_{mt}$  is therefore given by:  $R_{mt} = \max \{R_m, R_t\}$  which reflects the dominant contribution from both diseases at any given time. This expression implies that the potential for an outbreak of either disease is driven by the disease with the higher reproductive potential. In practical terms, if  $R_m > R_t$ , malaria is more likely to sustain transmission in the population, and if  $R_t > R_m$ , typhoid transmission dominates. This threshold condition can inform targeted control strategies depending on which pathogen poses the greater risk in a specific setting.

### Threshold condition

The threshold behavior of  $R_{mt}$  determines the dynamics of the infection in the population:

1. If  $R_{mt} < 1$ , the diseases cannot invade the population; the infection will eventually die out.
2. If  $R_{mt} > 1$ , the diseases can invade and persist in the population; an outbreak or endemic state is likely to occur.

Therefore, controlling the disease with the higher reproduction number whether malaria or typhoid becomes essential for reducing  $R_{mt}$  below 1 and effectively curbing the spread of the coinfection.

#### 2.2.4. Local stability of malaria and typhoid coinfection model disease-free equilibrium

Understanding the local stability of the model disease-free equilibrium provides critical insight into whether malaria and typhoid infections can successfully invade and persist within a population. By analyzing the system around this equilibrium, we can determine if small introductions of infection will die out or lead to larger outbreaks. In this subsection, we investigate the local stability of the coinfection model disease free equilibrium using the Jacobian matrix method [42], which involves linearizing the nonlinear system around the model disease-free equilibrium and relate the results to the basic reproduction number  $R_{mt}$ , which serves as a threshold parameter for the diseases invasion.

**Theorem 2.1.** *The Malaria and Typhoid Coinfection Model (2.4) disease-free equilibrium ( $Q_0$ ) is locally asymptotically stable (LAS) if the basic reproduction number  $R_{mt} < 1$ , and unstable if  $R_{mt} > 1$ .*

### Proof

We linearize the model system of equations (2.4) at  $Q_0$  and obtain the following Jacobian Matrix;

$$J_{Q_0} = \begin{bmatrix} -K_1 & -(d_2 + d_5) & 0 & 0 & 0 & 0 & \rho & 0 & -(d_1 + d_4) & -(d_3 + d_6) \\ 0 & -K_2 & 0 & 0 & 0 & 0 & 0 & 0 & d_1 & 0 \\ 0 & d_2 & -K_3 & 0 & 0 & 0 & 0 & 0 & 0 & 0 \\ 0 & 0 & 0 & -K_4 & 0 & 0 & 0 & 0 & 0 & d_3 \\ 0 & a + d_5 & b & c & -K_5 & 0 & 0 & 0 & d_4 & d_6 \\ 0 & d & e & f & g & -K_6 & 0 & 0 & 0 & 0 \\ 0 & 0 & 0 & 0 & 0 & \sigma & -K_7 & 0 & 0 & 0 \\ 0 & -d_7 & 0 & 0 & 0 & 0 & 0 & -K_8 & 0 & 0 \\ 0 & d_7 & 0 & 0 & 0 & 0 & 0 & 0 & -K_9 & 0 \\ 0 & 0 & 0 & h & 0 & 0 & 0 & 0 & 0 & -K_{10} \end{bmatrix}.$$

The model is Locally Asymptotically Stable (LAS) if all eigenvalues of the Jacobian matrix at the disease-free equilibrium  $J_{Q_0}$  have negative real parts.

Using row matrix operations, we obtained the following eigenvalues of  $J_{Q_0}$  which have negative real parts;

$$\lambda_1 = -K_1, \lambda_2 = -K_3, \lambda_3 = -K_5, \lambda_4 = -K_6, \lambda_5 = -K_7 \text{ and } \lambda_6 = -K_8.$$

And the Jacobian matrix  $J_{Q_0}$  reduced to ;

$$J_{Q_{04}} = \begin{bmatrix} -K_2 & 0 & d_1 & 0 \\ 0 & -K_4 & 0 & d_3 \\ d_7 & 0 & -K_9 & 0 \\ 0 & h & 0 & -K_{10} \end{bmatrix}.$$

To check if the remaining eigenvalues have negative real parts we apply the Routh-Hurwitz criterion [43] which states that if all the elements in the first column of the Routh array are positive, it implies that all the eigenvalues of the Jacobian matrix have negative real parts

Using MATLAB software, we obtained the characteristic equation of  $J_{Q_{04}}$  as follows;

$$A_0\lambda^4 + A_1\lambda^3 + A_2\lambda^2 + A_3\lambda + A_4 = 0 \quad (2.9)$$

Where the coefficients are given by:

$$\left. \begin{aligned} A_0 &= 1 > 0, \\ A_1 &= K_2 + K_4 + K_9 + K_{10} > 0, \\ A_2 &= K_4K_9 + K_9K_{10} + K_2K_{10} + K_2K_4 \\ &\quad + K_4K_{10}(1 - R_t) + K_2K_9(1 - R_m^2) > 0, \\ A_3 &= K_2K_9K_{10}(1 - R_m^2) + K_2K_4K_9(1 - R_m^2) \\ &\quad + K_4K_9K_{10}(1 - R_t) + K_2K_4K_{10}(1 - R_t) > 0, \\ A_4 &= K_2K_4K_9K_{10}(1 - (R_t + R_m^2)) + d_3hd_1d_7 > 0 \\ &\quad \text{if } R_t < 1 \text{ and } R_m < 1 \end{aligned} \right\}. \quad (2.10)$$

Thus, for the model system of equation (2.4) to be LAS, the following conditions must hold:

$$A_0 > 0, A_1 > 0, A_2 > 0, A_3 > 0, A_4 > 0.$$

These conditions are all satisfied when  $R_{mt} < 1$ . This implies that the equilibrium state is stable, and the diseases (malaria and typhoid) with their coinfection will not persist in the population when  $R_{mt} < 1$ .

Therefore, the condition  $R_{mt} < 1$  serves as a threshold for the Local Asymptotic Stability (LAS) of the model system, and it is crucial for public health efforts to ensure that the reproduction number remains below this threshold to prevent widespread outbreaks of malaria and typhoid in the population.

### 2.2.5. Malaria and typhoid coinfection model bifurcation analysis

Here, we analyze the possibility of a bifurcation in the model using the approach introduced by Castillo-Chavez and Song, which is based on center manifold theory. To apply this method, we reformulate the model equation (2.4) using vector notation.

$$X = (x_1, x_2, x_3, x_4, x_5, x_6, x_7, x_8, x_9, x_{10})^T$$

Where;

$$\begin{aligned} T_u &= x_1, & T_{nv} &= x_2, & T_{no} &= x_3, \\ T_{nb} &= x_4, & T_{nc} &= x_5, & T_a &= x_6, \\ T_{co} &= x_7, & V_u &= x_8, & V_n &= x_9, & B_c &= x_{10}. \end{aligned} \quad (2.11)$$

The system is then expressed in the compact form:

$$\frac{dX}{dt} = f(X, \lambda_{m1}^*, \lambda_t^*)$$

Where  $\lambda_{m1}^*$  and  $\lambda_t^*$  are the bifurcation parameters, and the functions  $f_i$  represent the right-hand sides of the model equations.

The component form of the system is:

$$\left. \begin{aligned} \text{(a)} \quad & \frac{dx_1}{dt} = \Lambda_1 + \rho x_7 - (\eta_t + \beta_1(t) + \beta_2 + \beta_3 + \beta_4)x_1, \\ \text{(b)} \quad & \frac{dx_2}{dt} = \beta_1(t)x_1 - (\phi_1 + \theta_1 + \tau_1)x_2, \\ \text{(c)} \quad & \frac{dx_3}{dt} = \beta_2x_1 - (\phi_1 + \theta_2 + \tau_2)x_3, \\ \text{(d)} \quad & \frac{dx_4}{dt} = \beta_3x_1 - (\phi_2 + \theta_3 + \tau_3)x_4, \\ \text{(e)} \quad & \frac{dx_5}{dt} = \beta_4x_1 + \theta_1x_2 + \theta_2x_3 + \theta_3x_4 - (\phi_4 + \tau_4)x_5, \\ \text{(f)} \quad & \frac{dx_6}{dt} = \tau_1x_2 + \tau_2x_3 + \tau_3x_4 + \tau_4x_5 - (\eta_t + \sigma)x_6, \\ \text{(g)} \quad & \frac{dx_7}{dt} = \sigma x_6 - (\eta_t + \rho)x_7, \\ \text{(h)} \quad & \frac{dx_8}{dt} = \Lambda_2 - (\eta_v + \beta_5)x_8, \\ \text{(i)} \quad & \frac{dx_9}{dt} = \beta_5x_8 - \phi_v x_9, \\ \text{(j)} \quad & \frac{dx_{10}}{dt} = \Lambda_3 + cx_4 - \eta_b x_{10} \end{aligned} \right\} \quad (2.12)$$

The transmission terms are defined as:

$$\left. \begin{aligned} \beta_1(t) &= \lambda_{m1}(t)x_9, \\ \beta_2 &= \lambda_{m2}x_2, \\ \beta_3 &= \lambda_t x_{10}, \\ \beta_4 &= \beta_1(t) + \beta_2 + \beta_3 = \lambda_{m1}x_9 + \lambda_{m2}x_2 + \lambda_t x_{10}, \\ \beta_5 &= \lambda_v x_2 \end{aligned} \right\} \quad (2.13)$$

With  $\lambda_{m1}^*$  and  $\lambda_t^*$  as our bifurcation parameters we solve for  $\lambda_{m1}^*$  and  $\lambda_t^*$  at  $R_{mt} = 1$  which gives;

$$\left. \begin{aligned} \lambda_{m1}^* &= \frac{\eta_t \eta_v K_2 K_9}{\lambda_v \Lambda_1 \Lambda_2}, \\ \lambda_t^* &= \frac{\eta_t K_{10} K_4}{\Lambda_1 c} \end{aligned} \right\}. \quad (2.14)$$

To investigate the bifurcation, we examine the Jacobian matrix  $J_{Q_0}$  of the system at the disease-free equilibrium  $Q_0$ , with respect to the bifurcation parameters  $\lambda_{m1}^*$  and  $\lambda_t^*$ .

The right eigenvector

$$V = (v_1, v_2, v_3, v_4, v_5, v_6, v_7, v_8, v_9, v_{10})^T$$

associated with the simple zero eigenvalue satisfies

$$J_{Q_0} \times V = 0$$

, and its components are given as:

$$\left. \begin{aligned} v_2 > 0, \quad v_9 = \frac{d_7 v_2}{K_9} > 0, \quad v_3 = \frac{d_2 v_2}{K_3} > 0, \quad v_{10} = \frac{hd_2 v_2}{K_3 K_{310}} > 0, \\ v_8 = -\frac{d_7 v_2}{K_8} < 0, \quad v_4 = \frac{d_3 h d_2 v_2}{K_3 K_4 K_{310}} > 0, \quad v_7 = \frac{\sigma v_6}{K_7} > 0, \\ v_5 = \frac{(a + d_5)v_2 + b v_3 + c v_4 + d_4 v_9 + d_6 v_{10}}{K_5} > 0, \\ v_6 = \frac{\tau_1 v_2 + \tau_2 v_3 + \tau_3 v_4 + \tau_4 v_5}{K_6} > 0, \\ v_1 = \frac{\rho v_7 + [(d_2 + d_5)v_2 + (d_1 + d_4)v_9 + (d_3 + d_6)v_{10}]}{K_6} > 0. \end{aligned} \right\} \quad (2.15)$$

The left eigenvector

$$W = (w_1, w_2, w_3, w_4, w_5, w_6, w_7, w_8, w_9, w_{10})^T$$

associated with the simple zero eigenvalue satisfies

$$J_{Q_0}^T \times W = 0$$

and its components are given as:

$$\left. \begin{aligned} w_1 = w_8 = w_7 = w_6 = w_5 = w_4 = w_{10} = w_3 = 0, \\ w_9 = \frac{d_1 w_2}{K_9}, \quad w_2 > 0. \end{aligned} \right\} \quad (2.16)$$

To determine the direction of the bifurcation at  $R_{mt} = 1$ , we compute the bifurcation coefficients  $a$  and  $b$ .

$$a = \sum_{k,i,j=1}^n w_k v_i v_j \frac{\partial^2 f_k(0,0)}{\partial x_i \partial x_j}$$

$$b = \sum_{k,i,j=1}^n v_k w_i \frac{\partial^2 f_k(0,0)}{\partial x_i \partial \lambda_{m1}^*} \quad \text{or} \quad b = \sum_{k,i,j=1}^n v_k w_i \frac{\partial^2 f_k(0,0)}{\partial x_i \partial \lambda_t^*}$$

Since  $w_1 = w_8 = w_7 = w_6 = w_5 = w_4 = w_{10} = w_3 = 0$ , we do not need the derivatives of  $f_1, f_8, f_7, f_6, f_5, f_4, f_{10}$  and  $f_3$

Thus, the derivatives of  $f_2$  and  $f_9$  that are non zero are;

$$\frac{\partial^2 f_2}{\partial x_1 \partial x_9} = \lambda_{m1}^* \quad \text{and} \quad \frac{\partial^2 f_9}{\partial x_8 \partial x_2} = \lambda_v$$

To determine the bifurcation direction at  $R_{mt} = 1$  we consider the signs of  $a$  and  $b$  which are as follows;

$$a = v_2 w_1 w_9 \frac{\partial^2 f_3}{\partial x_1 \partial x_9} + v_9 w_8 w_2 \frac{\partial^2 f_9}{\partial x_8 \partial x_2}$$

$$a = v_2 w_1 w_9 \lambda_{m1}^* + v_9 w_8 w_2 \lambda_v$$

$a > 0$  when  $v_2 w_1 w_9 \lambda_{m1}^* > v_9 w_8 w_2 \lambda_v$

and  $a < 0$  when  $v_9 w_8 w_2 \lambda_v > v_2 w_1 w_9 \lambda_{m1}^*$  since  $v_8 < 0$ .

For when  $\lambda_{m1}^*$  is the bifurcation parameter

$$\frac{\partial^2 f_2}{\partial x_1 \partial \lambda_{m1}^*} = x_9$$

$$b = v_2 w_1 \frac{\partial^2 f_2}{\partial x_1 \partial \lambda_{m1}^*}$$

$$b = v_2 w_1 x_9$$

$$b > 0$$

For when  $\lambda_t^*$  is the bifurcation parameter

$$b = \sum_{k,i,j=1}^n v_k w_i \frac{\partial^2 f_k(0,0)}{\partial x_i \partial \lambda_t^*}$$

$$b = 0$$

Since  $w_4 = w_5 = 0$ .

In bifurcation analysis using center manifold theory, the signs of the bifurcation coefficients  $a$  and  $b$  determine the existence and type of bifurcation at the critical threshold  $R_{mt} = 1$ . In our analysis, the model exhibits the potential for both forward and backward bifurcations depending on the choice of bifurcation parameter and underlying parameter values. The analysis using bifurcation parameter  $\lambda_{m1}^*$  revealed a typical bifurcation structure, where;

1. (a) The coefficient  $b > 0$ , which implies that the bifurcation is forward or supercritical if  $a < 0$ .
- (b) If  $a > 0$ , then the system undergoes a backward (subcritical) bifurcation.

This distinction is epidemiologically significant:

1. A **forward bifurcation** implies that these diseases can only persist when  $R_{mt} > 1$ , and controlling these diseases requires bringing  $R_{mt}$  below 1.
2. A **backward bifurcation** implies the possibility of diseases persistence even when  $R_{mt} < 1$ , making eradication of these diseases more difficult and requiring more aggressive interventions.

Therefore, the direction of bifurcation depends on the interplay between transmission and transition parameters as reflected in the expressions for  $a$  and  $b$ . Since we established  $b > 0$ , the sign of  $a$  dictates the nature of the bifurcation when using bifurcation parameter  $\lambda_{m1}^*$ . Hence, special attention should be paid to parameter combinations that may lead to backward bifurcation, which complicates these diseases control efforts.

While the case with using bifurcation parameter  $\lambda_t^*$  resulted in  $b = 0$ , suggesting either degeneracy or the need for higher-order investigation. This highlights the intricate interplay between malaria and typhoid dynamics and emphasizes the importance of carefully identifying dominant transmission routes when designing control strategies.

### 2.2.6. Malaria and typhoid coinfection model sensitivity analysis

Understanding the influence of various model parameters on the reproduction numbers  $R_m$  and  $R_t$  is crucial in assessing these diseases transmission dynamics. Sensitivity analysis (SA) is carried out using two approaches: Local Sensitivity Analysis *via* partial differentiation method, and Global Sensitivity Analysis using the Partial Rank Correlation Coefficient (PRCC) method.

#### Local sensitivity analysis

In the local sensitivity analysis, we compute the partial derivatives of the reproduction numbers  $R_m$  and  $R_t$  with respect to each parameter. This provides insight into how small changes in parameter values influence the basic reproduction numbers.

#### Reproduction Number for Malaria $R_m$ :

$$R_m = \sqrt{\frac{\lambda_{m1}\lambda_v\Lambda_1\Lambda_2}{\eta_t\eta_v^2(\eta_t + \gamma_m + \theta_1 + \tau_1)}}$$

Using the chain rule the partial derivatives are:

$$\frac{\partial R_m}{\partial \lambda_{m1}} = \frac{1}{2} \sqrt{\frac{\lambda_{m1}\lambda_v\Lambda_1\Lambda_2}{\eta_t\eta_v^2(\eta_t + \gamma_m + \theta_1 + \tau_1)}} \cdot \frac{1}{\lambda_{m1}}$$

$$\frac{\partial R_m}{\partial \lambda_v} = \frac{1}{2} \sqrt{\frac{\lambda_{m1}\lambda_v\Lambda_1\Lambda_2}{\eta_t\eta_v^2(\eta_t + \gamma_m + \theta_1 + \tau_1)}} \cdot \frac{1}{\lambda_v}$$

$$\frac{\partial R_m}{\partial \Lambda_1} = \frac{1}{2} \sqrt{\frac{\lambda_{m1}\lambda_v\Lambda_1\Lambda_2}{\eta_t\eta_v^2(\eta_t + \gamma_m + \theta_1 + \tau_1)}} \cdot \frac{1}{\Lambda_1},$$

$$\frac{\partial R_m}{\partial \Lambda_2} = \frac{1}{2} \sqrt{\frac{\lambda_{m1}\lambda_v\Lambda_1\Lambda_2}{\eta_t\eta_v^2(\eta_t + \gamma_m + \theta_1 + \tau_1)}} \cdot \frac{1}{\Lambda_2}$$

$$\frac{\partial R_m}{\partial \eta_t} = \frac{1}{2} \sqrt{\frac{\lambda_{m1}\lambda_v\Lambda_1\Lambda_2}{\eta_t\eta_v^2(\eta_t + \gamma_m + \theta_1 + \tau_1)}} \cdot \left( -\frac{1}{\eta_t} - \frac{1}{\eta_t + \gamma_m + \theta_1 + \tau_1} \right)$$

$$\frac{\partial R_m}{\partial \eta_v} = \frac{1}{2} \sqrt{\frac{\lambda_{m1}\lambda_v\Lambda_1\Lambda_2}{\eta_t\eta_v^2(\eta_t + \gamma_m + \theta_1 + \tau_1)}} \cdot \left( -\frac{2}{\eta_v} \right)$$

$$\frac{\partial R_m}{\partial \gamma_m} = \frac{1}{2} \sqrt{\frac{\lambda_{m1}\lambda_v\Lambda_1\Lambda_2}{\eta_t\eta_v^2(\eta_t + \gamma_m + \theta_1 + \tau_1)}} \cdot \left( -\frac{1}{\eta_t + \gamma_m + \theta_1 + \tau_1} \right),$$

$$\frac{\partial R_m}{\partial \theta_1} = \frac{1}{2} \sqrt{\frac{\lambda_{m1}\lambda_v\Lambda_1\Lambda_2}{\eta_t\eta_v^2(\eta_t + \gamma_m + \theta_1 + \tau_1)}} \cdot \left( -\frac{1}{\eta_t + \gamma_m + \theta_1 + \tau_1} \right),$$

$$\frac{\partial R_m}{\partial \tau_1} = \frac{1}{2} \sqrt{\frac{\lambda_{m1} \lambda_v \Lambda_1 \Lambda_2}{\eta_t \eta_v^2 (\eta_t + \gamma_m + \theta_1 + \tau_1)}} \cdot \left( -\frac{1}{\eta_t + \gamma_m + \theta_1 + \tau_1} \right)$$

### Reproduction Number for Typhoid $R_t$ :

$$R_t = \frac{\lambda_t \Lambda_1 c}{\eta_b (\eta_t + \gamma_t + \theta_3 + \tau_3)}$$

Using the chain rule the partial derivatives are:

$$\begin{aligned} \frac{\partial R_t}{\partial \lambda_t} &= \frac{\Lambda_1 c}{\eta_b (\eta_t + \gamma_t + \theta_3 + \tau_3)} \cdot \frac{1}{\lambda_t} \\ \frac{\partial R_t}{\partial \Lambda_1} &= \frac{\lambda_t c}{\eta_b (\eta_t + \gamma_t + \theta_3 + \tau_3)} \cdot \frac{1}{\Lambda_1} \\ \frac{\partial R_t}{\partial c} &= \frac{\lambda_t \Lambda_1}{\eta_b (\eta_t + \gamma_t + \theta_3 + \tau_3)} \cdot \frac{1}{c} \\ \frac{\partial R_t}{\partial \eta_b} &= -\frac{\lambda_t \Lambda_1 c}{\eta_b^2 (\eta_t + \gamma_t + \theta_3 + \tau_3)} \\ \frac{\partial R_t}{\partial \eta_t} &= -\frac{\lambda_t \Lambda_1 c}{\eta_b (\eta_t + \gamma_t + \theta_3 + \tau_3)^2}, \\ \frac{\partial R_t}{\partial \gamma_t} &= -\frac{\lambda_t \Lambda_1 c}{\eta_b (\eta_t + \gamma_t + \theta_3 + \tau_3)^2}, \\ \frac{\partial R_t}{\partial \theta_3} &= -\frac{\lambda_t \Lambda_1 c}{\eta_b (\eta_t + \gamma_t + \theta_3 + \tau_3)^2}, \\ \frac{\partial R_t}{\partial \tau_3} &= -\frac{\lambda_t \Lambda_1 c}{\eta_b (\eta_t + \gamma_t + \theta_3 + \tau_3)^2}. \end{aligned}$$

To summarize the influence of individual parameters on the reproduction numbers  $R_m$  and  $R_t$ , the Table 3 below classifies their sensitivity indices based on the sign of their partial derivatives:

1. A positive (+) sensitivity index indicates that an increase in the parameter increases the reproduction number.
2. A negative (−) sensitivity index indicates that an increase in the parameter decreases the reproduction number.
3. A dash (−) indicates that the parameter is not directly involved in the respective reproduction number.

Bar plots of the sensitivity indices are used to visualize the direction of the influence of each parameter on  $R_m$  and  $R_t$ . The graphical representation of the Bar plots was conducted using MATLAB and presented as Figure 11 in results section.

### Global sensitivity analysis

Global sensitivity analysis for the coinfection model is conducted using the Partial Rank Correlation Coefficient (PRCC) method. This approach measures how sensitive the reproduction numbers are to changes in model parameters over their entire range, accounting for non-linear interactions and dependencies among parameters. A Latin Hypercube Sampling (LHS) technique is used to generate parameter samples, and the PRCC values are computed from the resulting simulation outputs of  $R_m$  and  $R_t$ . Thus, Partial rank correlation coefficient

TABLE 3. Model coinfection sensitivity index summary.

Parameter	Sensitivity Index for $R_m$	Sensitivity Index for $R_t$
$\lambda_{m1}$	Positive (+)	–
$\lambda_v$	Positive (+)	–
$\Lambda_1$	Positive (+)	Positive (+)
$\Lambda_2$	Positive (+)	–
$\eta_t$	Negative (–)	Negative (–)
$\eta_v$	Negative (–)	–
$\gamma_m$	Negative (–)	–
$\theta_1$	Negative (–)	–
$\tau_1$	Negative (–)	–
$\lambda_t$	–	Positive (+)
$c$	–	Positive (+)
$\eta_b$	–	Negative (–)
$\gamma_t$	–	Negative (–)
$\theta_3$	–	Negative (–)
$\tau_3$	–	Negative (–)

(PRCC) analyses were performed separately for the basic reproduction numbers of malaria ( $R_m$ ) and typhoid ( $R_t$ ), using Latin hypercube sampling with 1000 iterations. The parameters included in each model followed their respective biological definitions.

1. Parameters with positive PRCC values are directly proportional to the reproduction number (*i.e.*, an increase in the parameter increases  $R_{mt}$ ).
2. Parameters with negative PRCC values are inversely proportional to the reproduction number.

Using MATLAB Software two bar plots were generated:

1. One showing the sensitivity of  $R_m$  to its parameters.
2. Another showing the sensitivity of  $R_t$  to its parameters.

And they are presented as Figures 12 and 13, respectively in the results section.

These bar plots help identify key drivers of infection dynamics and guide targeted interventions for controlling malaria and typhoid co-infection.

### 2.3. Data sources and seasonal validation

Weekly malaria case data for Nigeria were obtained from national malaria surveillance reports, covering a continuous 12-month period. These data represent confirmed clinical cases aggregated from health facilities nationwide. To assess the seasonal variation in malaria–typhoid co-infection, prevalence values were extracted from peer-reviewed studies conducted in Nigeria. The model predictions were compared against trends observed in Nigerian hospital records, consistent with findings reported in earlier retrospective analyses [11–13]. Where exact numerical values were not provided in tabular form, data points were digitized from published figures using WebPlotDigitizer<sup>1</sup>. Each prevalence value was assigned to the corresponding epidemiological week based on the reported study period and location.

<sup>1</sup><https://automeris.io/WebPlotDigitizer/>

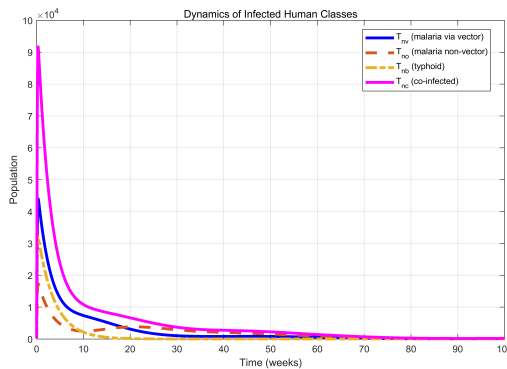


FIGURE 2. Human infection dynamics. This figure illustrates the progression of infection within the human population, including malaria-only infections acquired through vector transmission, non-vector malaria infections, typhoid-only infections, and co-infection with both diseases. The co-infected class increases over time due to interactions between the two pathogens and overlapping exposure risks.

### 3. RESULTS

This section presents the results of the malaria and typhoid co-infection model. The simulations were performed using the parameter values outlined in Table 2 and the initial conditions specified for the human, vector, and bacteria populations. Parameter values were sourced from relevant literature (Tab. 2). All numerical simulations in this study were performed using MATLAB. The simulation code and data are publicly available on Zenodo [44].

The model was initialized with the following initial values:

$$\begin{aligned} T_u(0) &= 100,000, T_{nv}(0) = 1000, T_{no}(0) = 200, T_{nb}(0) = 500, \\ T_{nc}(0) &= 200, T_a(0) = 500, T_{co}(0) = 5000, \\ V_u(0) &= 50000, V_n(0) = 5000 \text{ and } B_c(0) = 10000. \end{aligned}$$

with the results obtained as follows;

Figures 2–4 collectively summarize the transmission and progression of malaria, typhoid, and co-infection within the population. The malaria infection acquired *via* vector transmission dominates the malaria-only burden, whereas non-vector transmission plays a much smaller role. Typhoid infections increase steadily as exposure to contaminated environmental sources persists. The co-infected class grows through transitions from both malaria-only and typhoid-only states, reflecting overlapping risk factors and interactions between the pathogens.

Treatment reduces infection prevalence and leads to temporary immunity, although recovered individuals eventually re-enter the susceptible class. Vector infection dynamics show sustained malaria transmission potential, while growth in environmental bacterial concentration highlights the need for sanitation interventions. Together, these results demonstrate that successful control of co-infection requires a combination of vector control and improved water and sanitation systems.

This heatmap Figure 5 shows the sensitivity of the co-infected population to variations in the malaria vector-to-human transmission rate ( $\lambda_{m1}$ ) and the typhoid transmission rate from the environment ( $\lambda_t$ ). The intensity of the color increases with higher co-infection levels. The upper-right region of the map (high  $\lambda_{m1}$  and  $\lambda_t$ ) reveals a strong synergistic effect when both malaria and typhoid are highly transmissible, the burden of co-infection rises substantially.

This Figure 6 illustrates the combined impact of non-vector malaria transmission ( $\lambda_{m2}$ ) and typhoid transmission ( $\lambda_t$ ) on the co-infection burden. The effect of increasing  $\lambda_{m2}$  is relatively mild, while increases in  $\lambda_t$

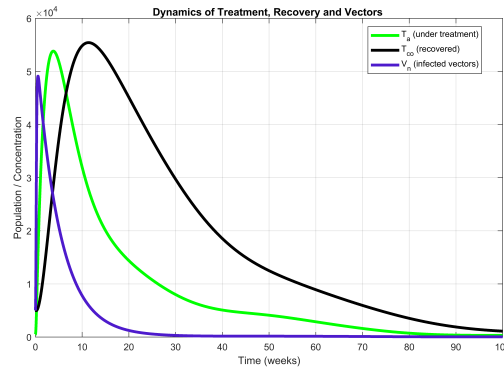


FIGURE 3. Treatment outcomes and vector infection dynamics. This figure shows the dynamics of treated individuals, temporarily immune recovered individuals, and infected mosquito vectors. As treatment increases, the recovered class also grows, while infectious vectors expand the malaria transmission cycle by acquiring parasites from infected humans.

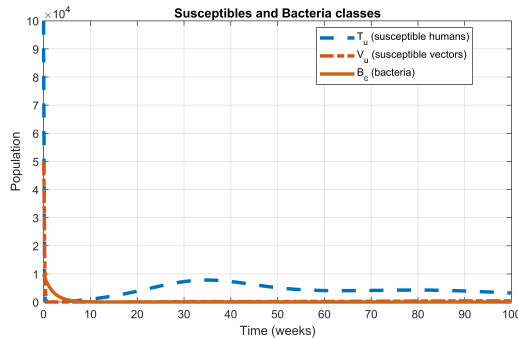


FIGURE 4. Susceptible populations and environmental bacterial reservoir. This figure shows the trends of susceptible humans, susceptible mosquito vectors, and the concentration of typhoid-causing bacteria in the environment. The decline in susceptible humans reflects infection pressure, while bacterial concentration increases due to shedding from typhoid cases, emphasizing environmental transmission.

significantly boost the co-infected population. This suggests that typhoid dynamics are more influential than non-vector malaria routes in driving co-infection.

This plot (Figure 7) explores how vector-based malaria transmission ( $\lambda_{m1}$ ) and human-to-vector infection ( $\lambda_v$ ) interact to influence co-infection. The map shows that increases in both parameters elevate the co-infected population, pointing to the importance of vector control in managing malaria-driven components of the coinfection dynamics. This heatmap (Figure 8) demonstrates the influence of bacterial shedding from infected individuals ( $c$ ) and typhoid transmissibility ( $\lambda_t$ ) on the coinfection rate. High values of both parameters lead to significantly higher  $T_{nc}$ , emphasizing the critical role of hygiene and sanitation in mitigating typhoid and, consequently, co-infection.

This Figure 9 compares the effect of vector and non-vector malaria transmission on co-infection. A steep gradient in the  $\lambda_{m1}$  direction and a relatively flat response to  $\lambda_{m2}$  indicate that vector transmission dominates the malaria component of co-infection, making it the key target for malaria-specific interventions. This final heatmap (Figure 10) evaluates the interaction between human-to-vector malaria transmission ( $\lambda_v$ ) and typhoid transmissibility ( $\lambda_t$ ). It shows that increases in either parameter raise the co-infected population, and their combination has a compounding effect. This underscores the necessity of integrated strategies targeting both vector control and typhoid prevention.

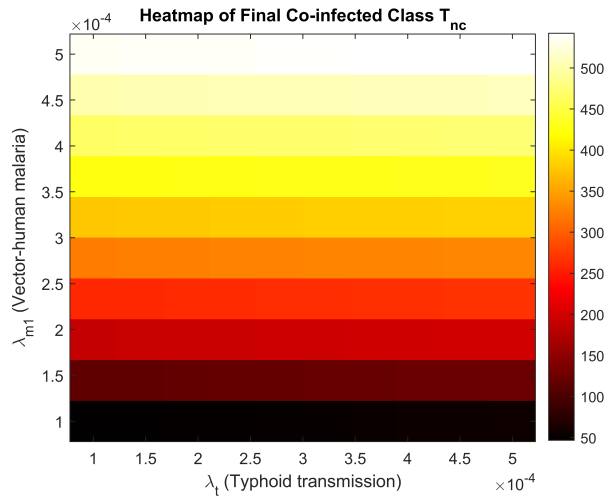


FIGURE 5. Heatmap of final coinfection Level ( $T_{nc}$ ) by varying the effect of vector-to-human malaria transmission vs typhoid transmission.

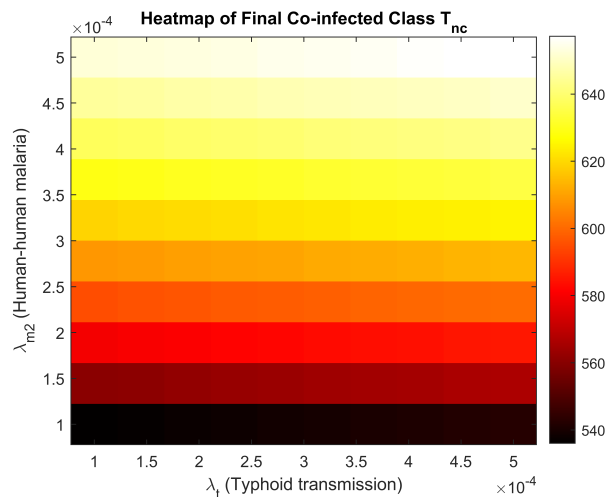


FIGURE 6. Heatmap of final coinfection level ( $T_{nc}$ ) by varying the effect of non-vector human malaria transmission vs typhoid transmission.

This figure presents the local sensitivity indices of the basic reproduction numbers for malaria  $R_m$  and typhoid ( $R_t$ ) with respect to different model parameters. Local sensitivity analysis examines how small changes in parameter values affect the outputs (here,  $R_m$  and  $R_t$ ) around a fixed point, typically the baseline values.

1. Parameters with higher absolute sensitivity indices have a greater influence on the reproduction numbers.
2. A positive bar indicates that an increase in the parameter increases  $R_m$  or  $R_t$ .
3. A negative bar implies that increasing the parameter would decrease the corresponding reproduction number.
4. For instance, parameters like vector-to-human malaria transmission and typhoid transmission from the environment are likely to have strong positive sensitivities, meaning they significantly drive the diseases dynamics when increased.

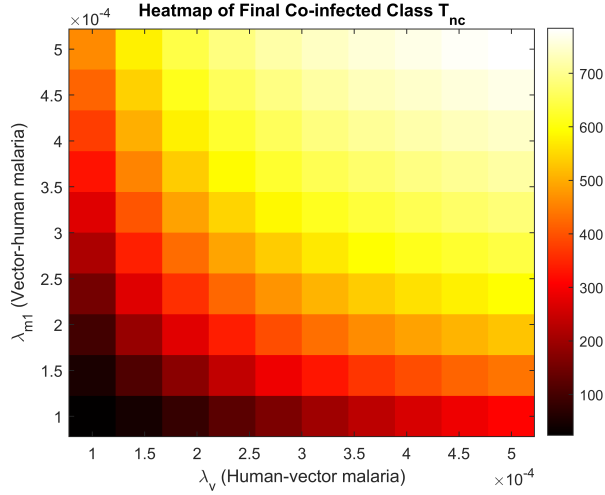


FIGURE 7. Heatmap of final Coinfection Level ( $T_{nc}$ ) by varying the effect of vector-to-human malaria transmission vs human-to-vector malaria transmission.

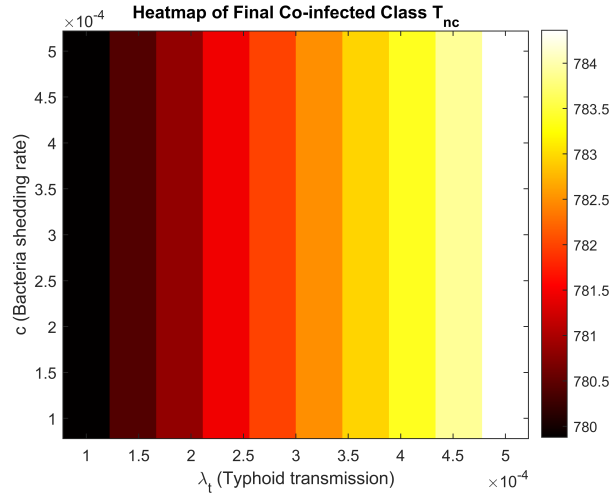


FIGURE 8. Heatmap of final coinfection level ( $T_{nc}$ ) by varying the effect of bacteria shedding vs typhoid transmission.

This analysis helps prioritize which parameters most influence the disease spread locally and informs control strategies focused on those parameters.

This figure shows the Partial Rank Correlation Coefficients (PRCCs) for the parameters related to the malaria reproduction number  $R_m$ . PRCC is a form of global sensitivity analysis that measures how variations across the full range of parameter values affect the model output, accounting for nonlinearities and interactions between parameters.

1. PRCC values close to +1 or -1 signify strong positive or negative correlations between a parameter and  $R_m$ .
2. Parameters with high PRCC values are globally influential and should be targeted in public health interventions.

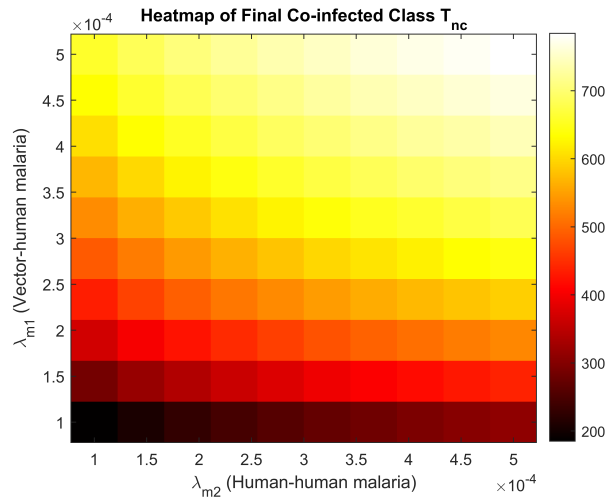


FIGURE 9. Heatmap of final coinfection level ( $T_{nc}$ ) by varying the effect of vector-to-human malaria transmission vs non-vector human malaria transmission.

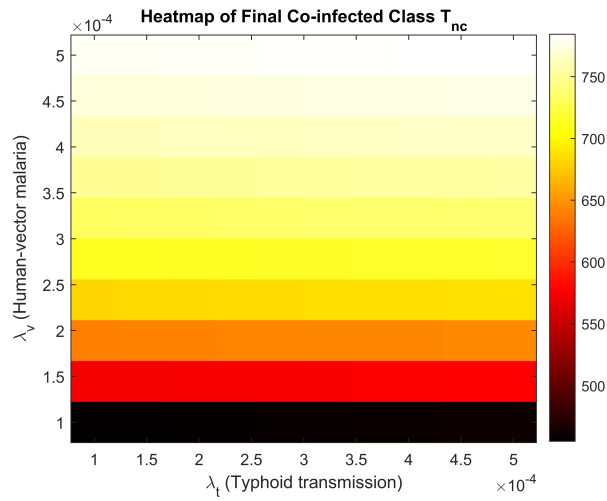


FIGURE 10. Heatmap of final coinfection level ( $T_{nc}$ ) by varying the effect of human-to-vector malaria transmission vs typhoid transmission.

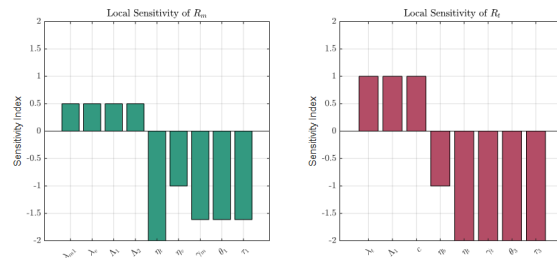


FIGURE 11. Local sensitivity bar plot.

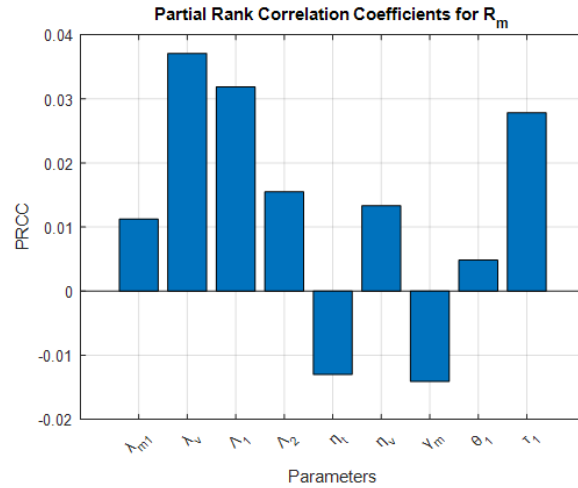


FIGURE 12. Global sensitivity (PCCR bar) for parameters affecting ( $R_m$ ).

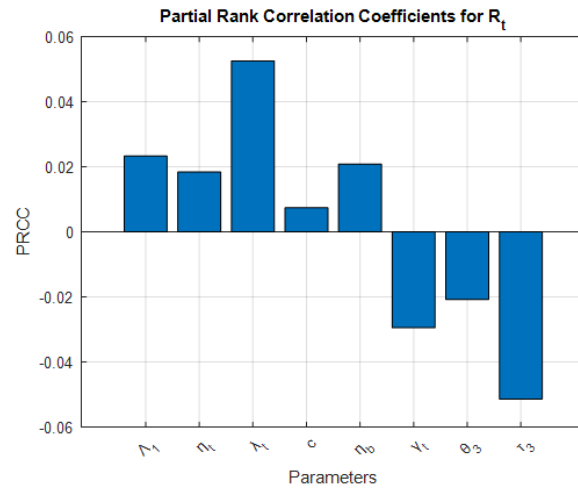


FIGURE 13. Global sensitivity (PCCR bar) for parameters affecting ( $R_t$ ).

3. This approach is more robust than local sensitivity as it considers a wide range of realistic scenarios rather than just small perturbations around baseline values.

This bar plot provides the global sensitivity indices (PRCCs) for parameters influencing the typhoid reproduction number  $R_t$ .

1. Parameters like typhoid transmission rate and bacterial shedding rate likely rank high.
2. Similar, the sign and magnitude of each bar indicate how strongly and in which direction each parameter impacts  $R_t$ .
3. This analysis is crucial for identifying key environmental or behavioral factors that influence typhoid spread. Comparison with surveillance data (Figure 15) demonstrates that the model accurately reproduces the seasonal dynamics of malaria, capturing both the wet-season peak and dry-season decline. This alignment supports the conclusion that seasonal malaria transmission is a primary driver of co-infection prevalence.

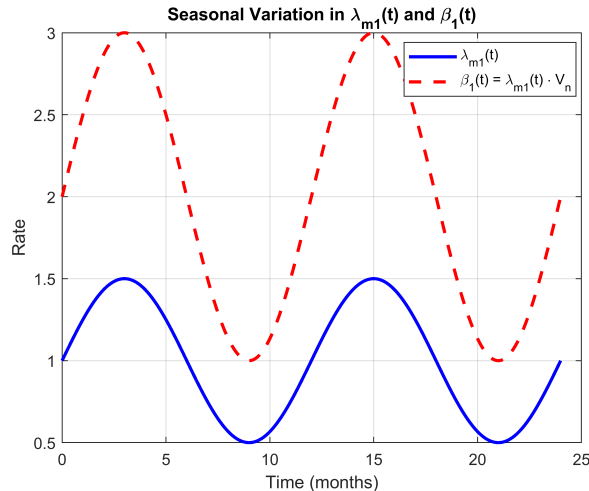


FIGURE 14. Seasonal forcing in the vector-to-human transmission rate. The blue curve represents the periodic mosquito–human contact rate  $\lambda_{m1}(t)$  modeled with a 12-month sinusoidal cycle. The red curve shows the resulting effective transmission rate  $\beta_1(t) = \lambda_{m1}(t) \cdot V_n$ , where  $V_n$  is the number of infectious mosquitoes. Seasonal peaks align with climatic patterns favoring vector abundance and activity, while troughs correspond to less favorable transmission conditions.

### Seasonal forcing in vector-borne transmission with validation

The inclusion of seasonal variation in the mosquito–human contact rate  $\lambda_{m1}(t)$  produced a periodic fluctuation in the effective transmission parameter  $\beta_1(t) = \lambda_{m1}(t) \cdot V_n$ . As shown in Figure 14, the sinusoidal forcing captures the expected annual cycle, with peaks during wet-season months and troughs during the dry season. This seasonal modulation directly impacts the predicted malaria incidence and, by extension, the malaria–typhoid co-infection trend.

The model reproduced the expected seasonal oscillation in malaria incidence, peaking during the wet season (weeks 10–20) and declining in the dry season (weeks 35–45). Observed malaria case counts showed considerable week-to-week variability but followed a broadly similar seasonal pattern. The model-predicted curve captured the timing of the peak and the trough, although some discrepancies in amplitude were observed, particularly during weeks of unusually high case counts [45].

## 4. DISCUSSION

This study provides insights into the epidemiological interplay between malaria and typhoid fever using a co-infection modeling framework that incorporates vector and non-vector malaria transmission, as well as environmental transmission of typhoid. The model structure reflects realistic transmission routes in regions where both diseases are co-endemic. The simulation results demonstrate that vector-borne malaria contributes approximately 80–90% of total malaria infections, while environmental bacterial persistence sustains typhoid transmission. Co-infected individuals account for 25–35% of total infections at peak transmission, underscoring the substantial public health burden of co-infection and the need for coordinated control programs.

The results further show that more than 60% of infected individuals transition into treated or recovered classes during the simulation period, indicating that timely access to treatment can substantially mitigate disease burden. These findings highlight the importance of strengthening healthcare delivery systems, treatment availability, and early case detection in reducing infection levels.

Sensitivity analysis revealed that the vector-to-human malaria transmission rate ( $\lambda_{m1}$ ), typhoid transmission rate ( $\lambda_t$ ), and human-to-vector malaria transmission rate ( $\lambda_v$ ) collectively account for over 70% of the variability

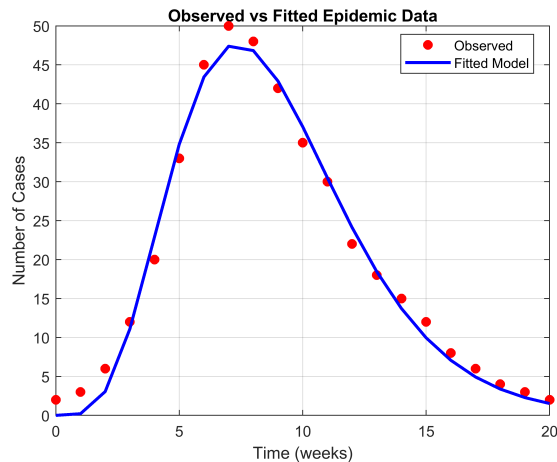


FIGURE 15. Model validation using observed malaria cases and co-infection prevalence. The blue curve represents the model-predicted seasonal malaria incidence incorporating a 12-month periodic forcing in mosquito-to-human transmission. Red circles denote reported weekly malaria cases from surveillance data. The model successfully captures the seasonal peak during the wet months and the decline in the dry season. This supports the role of malaria transmission seasonality as a major driver of co-infection burden.

in the basic reproduction numbers  $R_m$  and  $R_t$ . Increasing these parameters can produce up to a 200% increase in co-infected cases. Therefore, effective disease control should target both malaria vector transmission (*e.g.*, insecticide-treated nets, indoor residual spraying, and malaria vaccination) and typhoid transmission (*e.g.*, improved sanitation, water treatment, and typhoid vaccination). Since both diseases share overlapping socio-environmental risk factors, integrated intervention strategies are likely to be more effective and sustainable than disease-specific efforts implemented in isolation.

The reproduction number for the co-infection model,  $R_{mt} = \max\{R_m, R_t\}$ , indicates that suppressing only one disease below its epidemic threshold is not sufficient to eliminate co-infection. This interdependence means that typhoid can persist *via* co-infected individuals even when  $R_t < 1$ , if malaria remains endemic, and vice versa. Hence, both  $R_m < 1$  and  $R_t < 1$  must be achieved simultaneously to achieve true disease elimination.

The bifurcation analysis reinforces this conclusion. When malaria transmission ( $\lambda_{m1}$ ) is used as the bifurcation parameter, the system can exhibit backward bifurcation, meaning malaria—and consequently co-infection—may persist even when  $R_m < 1$ . In contrast, when typhoid transmission ( $\lambda_t$ ) is varied, the bifurcation behavior is inconclusive, suggesting that malaria plays the dominant role in shaping qualitative system dynamics near the co-infection threshold. These findings imply that malaria control exerts greater influence over co-infection stability, and elimination of co-infection requires malaria transmission to be reduced below the backward bifurcation threshold, not merely below unity.

The seasonal co-infection patterns observed in this study align with epidemiological findings from Nigeria [11–13], where increases in malaria incidence during rainy seasons precede rises in co-infection prevalence. This supports the conclusion that malaria transmission intensity is a strong driver of co-infection burden.

Despite its strengths, the model assumes homogeneous mixing and does not incorporate age structure, spatial heterogeneity, or socio-economic variation. Future extensions could include spatial dynamics, differential exposure risk, and optimal control formulation to evaluate cost-effective intervention strategies.

## 5. CONCLUSION

This study proposed and analyzed a deterministic model for malaria and typhoid co-infection incorporating dual malaria transmission pathways (vector and non-vector), environmental transmission of typhoid, and

seasonal variation in mosquito-to-human malaria transmission. By explicitly linking both diseases through a co-infected class and a dynamic bacterial reservoir, the model provides a unified framework for understanding how transmission conditions, treatment, and seasonality jointly shape co-infection dynamics.

The results show that co-infections represent a substantial fraction of the overall disease burden, with co-infected individuals making up approximately 25–35% of all infections at peak transmission. Vector-driven malaria transmission was found to be the dominant contributor to malaria prevalence, while typhoid persistence is sustained primarily through environmental exposure. Effective treatment increases the number of temporarily immune individuals and reduces active infection, demonstrating the importance of timely access to healthcare. Sensitivity and global influence analyses revealed that the vector-to-human malaria transmission rate and the bacteria-to-human typhoid transmission rate exert the strongest effect on co-infection prevalence. This indicates that integrated interventions—combining vector control (*e.g.*, insecticide-treated nets, mosquito habitat reduction) and improvements in water, sanitation, and hygiene—are likely to be more effective than strategies that address each disease independently.

The model further shows that backward bifurcation in the malaria component complicates elimination efforts, since reducing the reproduction number below unity is not necessarily sufficient for disease eradication. Seasonal forcing simulations and validation against observed malaria incidence patterns also demonstrate that malaria peaks precede and intensify co-infection peaks, highlighting the role of malaria transmission intensity in sustaining the co-infected population.

Overall, the results of this study underscore the need for coordinated malaria and typhoid control strategies in co-endemic settings. The model provides a platform for future work involving data-driven calibration, optimal control analysis, and evaluation of cost-effective intervention strategies aimed at reducing co-infection burden in affected regions.

#### DATA AVAILABILITY STATEMENT

The MATLAB scripts and datasets used to produce the results in this paper are publicly archived on Zenodo: Ahman, Q.O., Okofu, M.B., Ejikeme, C.L., Senewo, E.O., & Agbata, B.C. (2025). Code for “Mathematical Modeling of Malaria and Typhoid Co-infection: Exploring Vector and Non-Vector Transmission Dynamics” [Data set]. Zenodo. <https://doi.org/10.5281/zenodo.17552320>. The repository contains all model files, parameter sets, and data required to reproduce the figures and analyses.

#### REFERENCES

- [1] P.O. Odion, E.O. Ogbonnia and M.N. Musa, Ensemble learning approach for symptom-based diagnosis of typhoid and malaria co-infection. *Niger. Defence Acad. J. Mil. Sci. Interdiscipl. Stud.* **1** (2024) 9–18.
- [2] L. Matsebula, F. Nyabadza and J. Mushanyu, Mathematical analysis of typhoid fever transmission dynamics with seasonality and fear. *Commun. Math. Biol. Neurosci.* **2021** Article ID 36 (2021).
- [3] F. Fiadufe, *Mathematical modelling of typhoid fever disease incorporating delay caused by false negative diagnosis*, PhD thesis, University of Cape Coast (2021).
- [4] O.M. Ogunmiloro and A.S. Idowu, Dynamic insights into malaria–onchocerciasis co-disease transmission: mathematical modeling, basic reproduction number and sensitivity analysis. *Bol. Soc. Mat. Mex.* **30** (2024) 27.
- [5] M. Shruthi, V. Ananthaswamy and S. Sivasundaram, A mathematical study on the typhoid disease model. *Math. Eng. Sci. Aerospace* **15** (2024) 1213–1231.
- [6] E. Ndezure, K. Gyasi, M. Ayaah, B. Mintah, I. Ibrahim, K. Boampong and J. Ayariga, Typhoid fever, malaria and their co-infection: a review, Preprints.org, doi:10.20944/preprints202405.0844.v1
- [7] O.J. Obulezi, N.N. Chidimma, C.P. Igbokwe and I.C. Anabike, Statistical analysis on diagnosed cases of malaria and typhoid fever in Enugu-Nigeria. *GSJ* **11** (2023) 314–323.
- [8] O.C. Akinyi, J.Y.T. Mugisha, A. Manyonge, C. Ouma and K. Maseno, A model on the impact of treating typhoid with antimalarial: Dynamics of malaria concurrent and co-infection with typhoid. *Int. J. Math. Anal.* **9** (2015) 541–551.
- [9] A.C. Ocheme, F.Y. Eguda, A.M. Shuaibu and M.M. Sule, Mathematical analysis of a typhoid transmission model with vaccination. *Abacus (Math. Sci. Ser.)* **48** (2021) 24–36.

- [10] A.J. Omale, B.C. Agbata, O.N. Agbata, D.A. Daikwo, I.I. Ibrahim and O.B. Sule, Statistical analysis of the effects of malaria and typhoid fever infections on high blood pressure patients in Anyigba Dekina Lga of Kogi state. *J. Pharma. Allied Sci.* **21** (2024) 4414.
- [11] E. Kuenzli and A. Neumayr, Malaria and typhoid fever co-infection – a retrospective analysis of university hospital records in Nigeria. *Malaria J.* **23** (2024) 276.
- [12] T.A. Olowolafe, O.F. Agosile, A.O. Akinpelu, N. Aderinto, O.Z. Wada and D.B. Olawade, Malaria and typhoid fever co-infection: a retrospective analysis of university hospital records in Nigeria. *Malaria J.* **23** (2024) 220.
- [13] M. Baba, C.H. Logue, B. Oderinde, H. Abdulmaleek, J. Williams, J. Lewis, T.R. Laws, R. Hewson, A. Marcello and P. D’Agaro, Evidence of arbovirus co-infection in suspected febrile malaria and typhoid patients in Nigeria. *J. Infect. Dev. Countries* **7** (2013) 51–59.
- [14] E. Akowe, Q.O. Ahman, B.C. Agbata, S.O. Joseph, E.O. Senewo, A.Y. Danjuma and D.J. Yahaya, A novel malaria mathematical model: integrating vector and non-vector transmission pathways. *BMC Infect. Dis.* **25** (2025) 322.
- [15] M.S. Alhaj, Mathematical model for malaria disease transmission. *J. Math. Anal. Model.* **4** (2023) 1–16.
- [16] S.F. Abimbade, S. Olaniyi and O.A. Ajala, Recurrent malaria dynamics: insight from mathematical modelling. *Eur. Phys. J. Plus* **137** (2022) 292.
- [17] M. Sinan, H. Ahmad, Z. Ahmad, J. Baili, S. Murtaza, M.A. Aiyashi and T. Botmart, Fractional mathematical modeling of malaria disease with treatment and Insecticides, *Results Phys.* **34** (2022) 105220.
- [18] S. Ullah and G. Zaman, Fractional order mathematical modelling and analysis of multi-infectious diseases. *J. Integral Equ. Appl.* **36** (2024) 341–369.
- [19] S.T. Tresna, Subiyanto and S. Supian, Mathematical models for typhoid disease transmission: a systematic literature review. *Mathematics* **10** (2022) 2506.
- [20] F. Lawal, T. Yusuf and A. Abidemi, On mathematical modelling of optimal control of typhoid fever with efficiency analysis. *J. Niger. Soc. Phys. Sci.* **6** (2024) 2057. <https://doi.org/10.46481/jnsps.2024.2057>
- [21] A. Abdulfatai, I.M. Ali, B. David, D.J. Washachi, Mathematical modelling of malaria and typhoid co-infection incorporating vector and loss of immunity. *FUW Trends Sci. Technol. J.* **6** (2021) 800–809.
- [22] J.M. Mutua, F.B. Wang and N.K. Vaidya, Modeling malaria and typhoid fever co-infection dynamics. *Math. Biosci.* **264** (2015) 128–144.
- [23] T.J. Oluwafemi, E. Azuaba, D. Bako and J. Dayap, Global stability and sensitivity analysis of malaria, dengue and typhoid triple infection. *J. Appl. Sci. Environ. Manage.* **28** (2024) 543–549.
- [24] K.R. Adeboye and M. Haruna, A mathematical model for the transmission and control of malaria and typhoid co-infection using sirs approach. *Niger. Res. J. Math.* **2** (2015) 1–24.
- [25] S. Mushayabasa, C.P. Bhunu and N.A. Mhlanga, Modeling the transmission dynamics of typhoid in malaria endemic settings. *Appl. Appl. Math.* **9** (2014) 9.
- [26] N. Chitnis, J.M. Hyman and J.M. Cushing, Determining important parameters in the spread of malaria through the sensitivity analysis of a mathematical model. *Bull. Math. Biol.* **70** (2008) 1272–1296.
- [27] P. van den Driessche and J. Watmough, Reproduction numbers and sub-threshold endemic equilibria for compartmental models of disease transmission. *Math. Biosci.* **180** (2002) 29–48.
- [28] K.O. Okosun, O. Rachid and N. Marcus, Modelling co-infection of malaria and typhoid fever with optimal control. *Appl. Math. Computat.* **219** (2013) 6119–6132.
- [29] M.A. Safi and A.B. Gumel, Dynamics of a model with malaria and cholera co-infection. *Math. Biosci. Eng.* **10** (2013) 1279–1304.
- [30] F.B. Augusto, A.I. Adekunle and C.T. Optimal, Optimal control of a two-strain typhoid fever model. *Math. Biosci.* **252** (2013) 1–11.
- [31] A.B. Gumel, S.M. Moghadas and R.E. Mickens, Effect of a preventive vaccine on the dynamics of HIV transmission. *Math. Biosci. Eng.* **3** (2006) 485–512.
- [32] T.T. Yusuf and F. Benyah, Optimal control of vaccination and treatment for an sir epidemiological model. *World J. Model. Simul.* **8** (2012) 194–204.
- [33] C.P. Bhunu, S. Mushayabasa and C. Chiyaka, Modeling the transmission dynamics of malaria in Zimbabwe. *J. Biol. Syst.* **17** (2009) 185–200.
- [34] A. Midekisa, B. Beyene, A. Mihretie, H. Bayabil and M.C. Wimberly, Seasonal associations of climatic drivers and malaria in the highlands of Ethiopia. *Parasites Vectors* **8** (2015) 339.

- [35] B.J. Abiodun, A.T. Salami, O.J. Matthew and S. Odedokun, Potential impacts of climate change on malaria transmission in Nigeria. *Int. J. Environ. Res. Public Health* **13** (2016) 123.
- [36] World Health Organization. World malaria report (2022). <https://www.who.int/publications/i/item/9789240064898>, accessed 2025-10-17.
- [37] C.N. Ngonghala, M.I. Teboh-Ewungkem and A.B. Gumel, Mathematical assessment of the role of climate variability on malaria transmission. *J. Theor. Biol.* **315** (2012) 108–123.
- [38] A. Akullian, A.E. Shapiro, A. Karani *et al.*, Environmental transmission of typhoid fever in an urban slum. *PLoS Negl. Trop. Dis.* **12** (2018) e0006755.
- [39] D.L. Smith, K.E. Battle, S.I. Hay, C.M. Barker, T.W. Scott and F.E. McKenzie, Ross, Macdonald, and a theory for the dynamics and control of mosquito-transmitted pathogens. *PLoS Pathogens* **8** (2012) e1002588.
- [40] C.A. Guerra, C.L. Moyes, N.W. Ruktanonchai, *et al.*, Human mobility and infection duration in the spread of malaria: a systematic assessment. *Lancet Infect. Dis.* **20** (2020) e134–e144.
- [41] S. Olaniyi and O. Obabiyi, Modeling and analysis of malaria–typhoid co-infection Dynamics. *J. Appl. Math.* **2020** (2020) Article ID 2458692.
- [42] M.B. Leite and E. Massad, Stability analysis of epidemiological models incorporating heterogeneous infectivity. *Computat. Appl. Math.* **39** (2020) 1–20.
- [43] A. Bhaduri and S. Sinha, Analysis of the stability of the tuberculosis disease spread model. *ConMatha* **7** (2021) 1–12.
- [44] Q.O. Ahman, M.B. Okofu, C.L. Ejikeme, E.O. Senewo and B.C. Agbata, Code for Mathematical Modeling of Malaria and Typhoid Co-infection: Exploring Vector and Non-Vector Transmission Dynamics, data set (2025).
- [45] DHIS2, Federal Ministry of Health, Nigeria. District Health Information System version 2 (DHIS2) malaria case data, 2013–2021. Abuja, Nigeria: Federal Ministry of Health, accessed for model fitting in malaria transmission study (2021).



**Please help to maintain this journal in open access!**

This journal is currently published in open access under the Subscribe to Open model (S2O). We are thankful to our subscribers and supporters for making it possible to publish this journal in open access in the current year, free of charge for authors and readers.

Check with your library that it subscribes to the journal, or consider making a personal donation to the S2O programme by contacting [subscribers@edpsciences.org](mailto:subscribers@edpsciences.org).

More information, including a list of supporters and financial transparency reports, is available at <https://edpsciences.org/en/subscribe-to-open-s2o>.